



Comparative study of reactively and non-reactively sputtered high-entropy metal sublattice carbides

A. Kirnbauer^{a,*}, B.I. Hajas^a, S. Kolozsvári^b, P.H. Mayrhofer^a

^a Institute of Materials Science and Technology, TU Wien, A-1060 Vienna, Austria

^b Plansee Composite Materials GmbH, D-86983 Lechbruck am See, Germany

ARTICLE INFO

Keywords:

High-entropy ceramics
Chemically complex alloys
Thermal stability
Mechanical properties

ABSTRACT

Non-reactive (nr) as well as reactive (r) magnetron sputtering was utilised to compare the phase formation and mechanical properties of (Hf,Ta,Ti,V,Zr)-carbide coatings. The nr-synthesised coatings form a single-phase fcc-structured solid solution, whereas the r-synthesised ones show a strong dependence on the used acetylene flow ($f_{C_2H_2}$). Thereby, only the coating deposited with $f_{C_2H_2} = 20\%$ (the total flow is Ar + C₂H₂) exhibit a single-phase structure, whereas coatings deposited with lower acetylene flow rate ratio show partly XRD-amorphous patterns. The hardness comparison of the two single-phased coatings shows that the nr-sputtered one exhibits 41.6 ± 1.6 GPa, while the r-sputtered one is noticeably softer with 34.8 ± 1.6 GPa. Upon vacuum annealing of free-standing powdered coating materials, both show no structural change up to 1300 °C, only a reduction in their X-ray diffraction peak widths (indicative for structural relaxation effects). However, vacuum annealing of coated sapphire substrates at 1000–1300 °C caused spallation of the r-(Hf,Ta,Ti,V,Zr)C, while the nr-(Hf,Ta,Ti,V,Zr)C stayed intact, with an additional phase formed only when annealed at 1300 °C supposedly due to an interface reaction with the sapphire substrate. This nr-(Hf,Ta,Ti,V,Zr)C only slightly softens to 40.2 ± 2.1 GPa upon annealing to 1200 °C, while a further increase to 1300 °C causes a reduction to 34.0 ± 2.4 GPa, due to this interface reaction and recovery effects. These findings suggest that nr-(Hf,Ta,Ti,V,Zr)C offers superior phase stability, mechanical robustness, and resistance to high-temperature degradation over their reactively-prepared counterparts, making them better suited for applications demanding thermal stability and hardness retention.

1. Introduction

The utilisation of ceramic coatings deposited by physical vapour deposition is nowadays a very common way to protect tools and components from the degradation caused by mechanical or thermal load as well as their environment. In this regard TiN and (Ti,Al)N-based coatings have proven to be successful [1–4]. But especially at elevated temperatures, nitrides are pushed to their limits. Therefore, borides or carbides, which are so called ultra-high temperature ceramics (UHTCs), are used as protective coatings for applications requiring temperatures >1500 °C [5–7]. In this regard HfC, TaC, or (Hf,Ta)C—which exhibits with ~4200 °C the highest known melting point—are due to their high thermal stability and hardness suitable candidates to protect tools and components from mechanical and thermal load [8,9]. Additionally, to binary and ternary ceramics, also material combinations using more elements are used. Especially for (Ti,Al)-based nitrides, the addition of refractory transition metals such as Ta, Mo, Zr, or W, has shown to be

successful in enhancing the thermal stability and oxidation resistance as well as fracture toughness [10–18]. In recent years, also the addition of rare earth metals such as La and Ce also showed promising results regarding the oxidation resistance and thermal stability [19–21]. Furthermore, also the high-entropy concept, using 5 metals in equimolar concentration, has been applied to nitrides, borides, oxides, and carbides to further increase the thermal stability and the oxidation resistance of ceramic thin films [7,22–28]. Due to the fact that essentially only their metal-sublattice is high entropic, the more specific term “high-entropy sublattice nitrides” was coined [23]. The huge potential of such a material development concept has been shown also for bulk carbides by theoretical as well as experimental studies [29–35]. In the field of PVD coatings, nitrides based on the high-entropy concept have shown to be potential candidates to be used in industry as they outperform conventional nitrides. However, high-entropy sublattice carbide thin films in contrast are rarely investigated. In this study we investigate the influence of the deposition process (reactive and non-reactive) on the phase

* Corresponding author.

E-mail address: alexander.kirnbauer@tuwien.ac.at (A. Kirnbauer).

<https://doi.org/10.1016/j.surfcoat.2024.131645>

Received 5 November 2024; Received in revised form 4 December 2024; Accepted 6 December 2024

Available online 8 December 2024

0257-8972/© 2024 The Authors. Published by Elsevier B.V. This is an open access article under the CC BY license (<http://creativecommons.org/licenses/by/4.0/>).

formation and mechanical properties of (Hf,Ta,Ti,V,Zr)-carbide coatings.

2. Experimental methods

The investigated (Hf,Ta,Ti,V,Zr)C coatings were developed using magnetically unbalanced magnetron sputtering. The non-reactively sputtered coatings (for easier reading further referred to as nr-(Hf,TA,Ti,V,Zr)C) were synthesised using a modified Leybold Z400 magnetron sputtering system equipped with one 3" cathode. The target used for these depositions consists of HfC, TaC, TiC, VC, and ZrC in an equimolar (20 mol% each) concentration (Plansee Composite Materials GmbH). For the reactive sputter process a metallic target consisting of the respective metals in equiatomic composition was used. The base pressure before heating the substrates to 450 °C was 2×10^{-4} Pa. During the deposition, a constant bias voltage of -50 V was applied.

The reactively sputtered coatings (further referred to as r-(Hf,Ta,Ti,V,Zr)C) were synthesised in an in-house built magnetron sputter system (FRIDA), equipped with one 3" cathode and an acetylene (C_2H_2) gas supply. Various coatings are prepared through sputtering the HfTaTiVZr metallic target in an Ar and acetylene gas mixture, using acetylene flow rate ratios $f_{C_2H_2} = (C_2H_2)/(Ar + C_2H_2)$ of either 5, 10, or 20 %. The coatings were deposited on Si (100), sapphire (1-102), and thin iron foil substrates, which were ultrasonically cleaned in acetone and ethanol for 10 min each. Subsequently, the substrates were placed in a substrate holder and after reaching a base pressure of 3×10^{-4} Pa they were heated to 450 °C. From the coatings deposited on the iron foil, free-standing coating material was produced by dissolving the iron foil in nitric acid. The coating flakes obtained were ground to powder, which is used for further microstructural investigations and annealing treatments to avoid/minimise substrate interference.

X-ray diffraction (XRD) with a PANalytical XPert Pro MPD (0- θ diffractometer) holding a Cu- K_α ($\lambda = 1.54 \text{ \AA}$) radiation source was conducted for microstructural investigations. The grazing incidence measurements were carried out on a PANalytical Empyrean material

diffractometer with the same copper source, at a grazing angle of 3° and a scintillation detector (0D) equipped with a parallel plate collimator. The mechanical properties of the coatings were determined using an UMIS II nanoindentation system. For each sample, measurements with 40 indents and a force range of 5–35 mN were carried out. The analysis of the recorded load displacement curves was done after Oliver and Pharr [36].

Scanning electron microscopy (SEM) investigations were carried out in a FEI Quanta 200 SEM utilising a field emission gun (FEG) operated at an acceleration voltage of 10 keV. Detailed structural investigations using transmission electron microscopy (TEM) were done in a TECNAI F20 FEG-TEM operated at 200 keV. The respective TEM samples were prepared using a SCIOS II focused ion beam (FIB) facility. To gain information about the thermal stability of the coatings, powdered coating material as well as coatings on sapphire substrates were vacuum annealed at a temperature range of 900–1300 °C for 10 min each. Subsequently, the samples were investigated by XRD and nanoindentation.

3. Results and discussion

XRD results of r-(Hf,Ta,Ti,V,Zr)C coatings are presented in Fig. 1a. The patterns show that with $f_{C_2H_2} = 5 \%$ the coatings exhibit very small grains or even amorphous character indicated by a very broad peak in the diffraction angle range of 30 to 40° where a second peak is only slightly visible. With increasing acetylene flow, the structure becomes more crystalline but no fully developed single phase crystalline material is present. The peak at $\sim 34^\circ$ suggests carbide formation with partly amorphous or metallic contributions indicated by its asymmetric shape. Further increasing $f_{C_2H_2}$ to 20 % leads to a single phased face-centred cubic carbide structure. For better comparison, powdered free-standing coating material was produced (by depositing the coatings on iron foil and subsequently dissolving the substrate in nitric acid, see Experimental methods) and investigated by XRD. This allows the contribution of more coating material, again a well-developed single

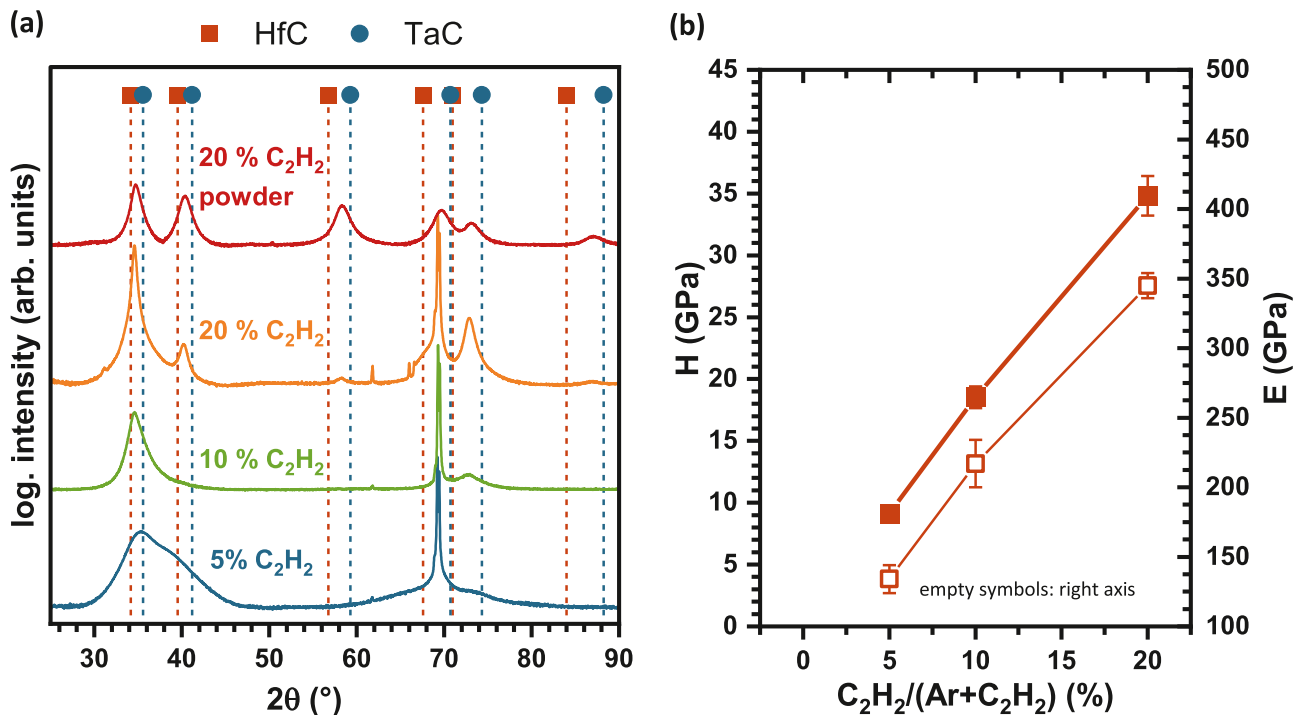


Fig. 1. (a) X-ray diffraction patterns of r-(Hf,Ta,Ti,V,Zr)C coatings on Si substrates depending on the acetylene flow rate ratio ($f_{C_2H_2}$) and powdered coating material deposited with $f_{C_2H_2} = 20 \%$. For comparison of the peak positions HfC (red squares, PDF #00-039-1491) and TaC (blue circles, PDF #00-035-0801) are indicated. (b) Hardness and indentation modulus of r-(Hf,Ta,Ti,V,Zr)C coatings depending on $f_{C_2H_2}$.

phase fcc structure is present, see Fig. 1a at the top. The lattice parameter of the powdered coating material is 4.47 Å (compare indicated HfC and TaC reference patterns). For the coatings on Si substrates the lattice parameter is 4.49 Å. The difference is due to the constraints with the substrate and suggests for growth-induced build-up of compressive stresses within the film. The differential thermal expansion between carbide and Si substrate would introduce tensile stresses upon cooling down from the deposition temperature. The thermally induced tensile stresses were calculated to be of ~ 0.8 GPa using an averaged thermal expansion coefficient from literature values of the binary ceramics and the biaxial E -modulus using the experimentally evaluated indentation modulus and an averaged Poisson's ratio of $\nu = 0.21$ [37]. The hardness and indentation modulus of the coatings deposited with the lowest acetylene flow rate ratio are 9.1 ± 0.3 GPa and 134 ± 10 GPa, respectively, see Fig. 1b. With increasing C_2H_2 flow rate the hardness increases to 18.5 ± 0.9 GPa (for the intermediate acetylene flow rate) and further to 34.8 ± 1.6 GPa (for the coating deposited with $f_{C_2H_2} = 20\%$). This fits very well to the observed structure. A similar behaviour can be observed for the indentation modulus, which increases to 217 ± 17 GPa for $f_{C_2H_2} = 10\%$ and then to 345 ± 9 GPa for the highest acetylene flow rate ratio. With a difference of 0.02 Å between the lattice parameters of the powdered free-standing coating material and the coating on the Si-substrate—which corresponds to a strain of $\sim 0.45\%$ —the residual compressive stress is therefore estimated to be ~ 2 GPa. Combining the thermally induced tensile stress and the residual compressive stresses, the intrinsic stress due to the deposition process yields -2.8 GPa. The trend of the hardness and the indentation modulus fits perfectly to the

structural results as their values reach the expected range for carbides as soon as the coating forms a well-developed single phased fcc carbide.

SEM fracture cross-section images of the coating deposited with $f_{C_2H_2} = 20\%$ show a very fine grained microstructure, which appears almost featureless, see Fig. 2a. TEM bright-field as well as dark-field images prove the fine grained microstructure and indicate columnar growth of the coating with column diameters of 20–50 nm (lengths of about 200 nm), see Fig. 2b and c. Selected area electron diffraction (SAED) patterns obtained from the area marked with a white dashed circle in Fig. 2b, further confirm the very fine structure due to the ring-like pattern, see Fig. 2d. The very small grains for the reactively deposited coatings stem from the combination of more random nucleation events during the film growth and the low ion energy, which leads to a more random distribution of the crystal orientations and a very fine-grained microstructure [38]. Furthermore, also here only contributions from the fcc phase can be identified, confirming the well-developed single-phase fcc structure as observed by XRD.

For comparison to the reactively prepared coatings, non-reactively prepared coatings of the same material system were developed. The SEM images in the case of the non-reactively prepared coatings show a columnar fracture cross section with much larger grains than those of the reactively deposited coatings, see Fig. 3a. The bright-field and dark-field TEM images confirm the columnar growth and the larger column size with diameters of 50–100 nm (with lengths in the order of ~ 1 μ m), see Fig. 3b and c. Therefore, the SAED pattern (using an aperture size of 500 nm diameter) exhibits rather discrete diffraction spots than continuous rings. Furthermore, from the SAED we can state that the non-

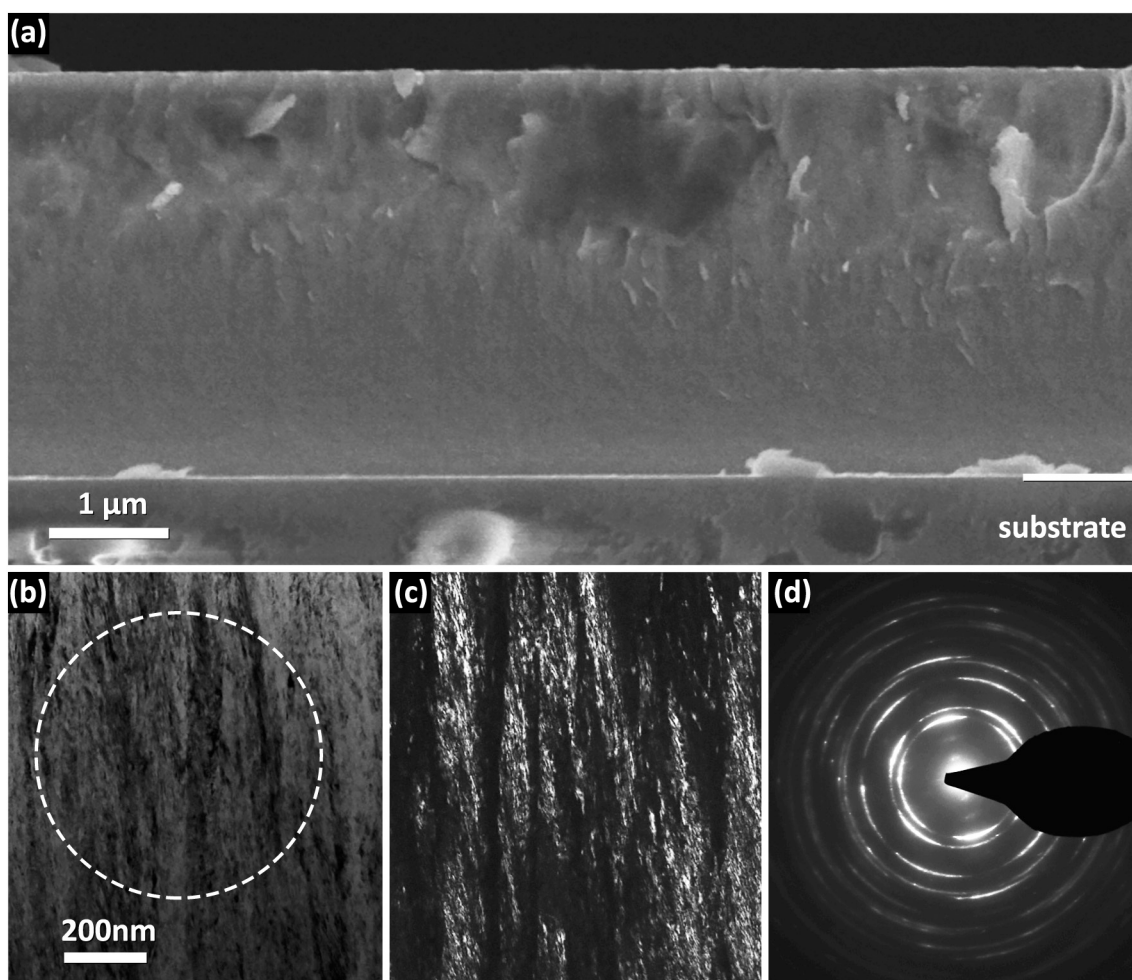


Fig. 2. Morphology of r -(Hf,Ta,Ti,V,Zr) carbide coatings deposited with $f_{C_2H_2} = 20\%$. (a) SEM fracture cross section, (b) TEM bright field image, (c) TEM dark field image, (d) SAED pattern taken from the area marked with a white dashed circle in (b).

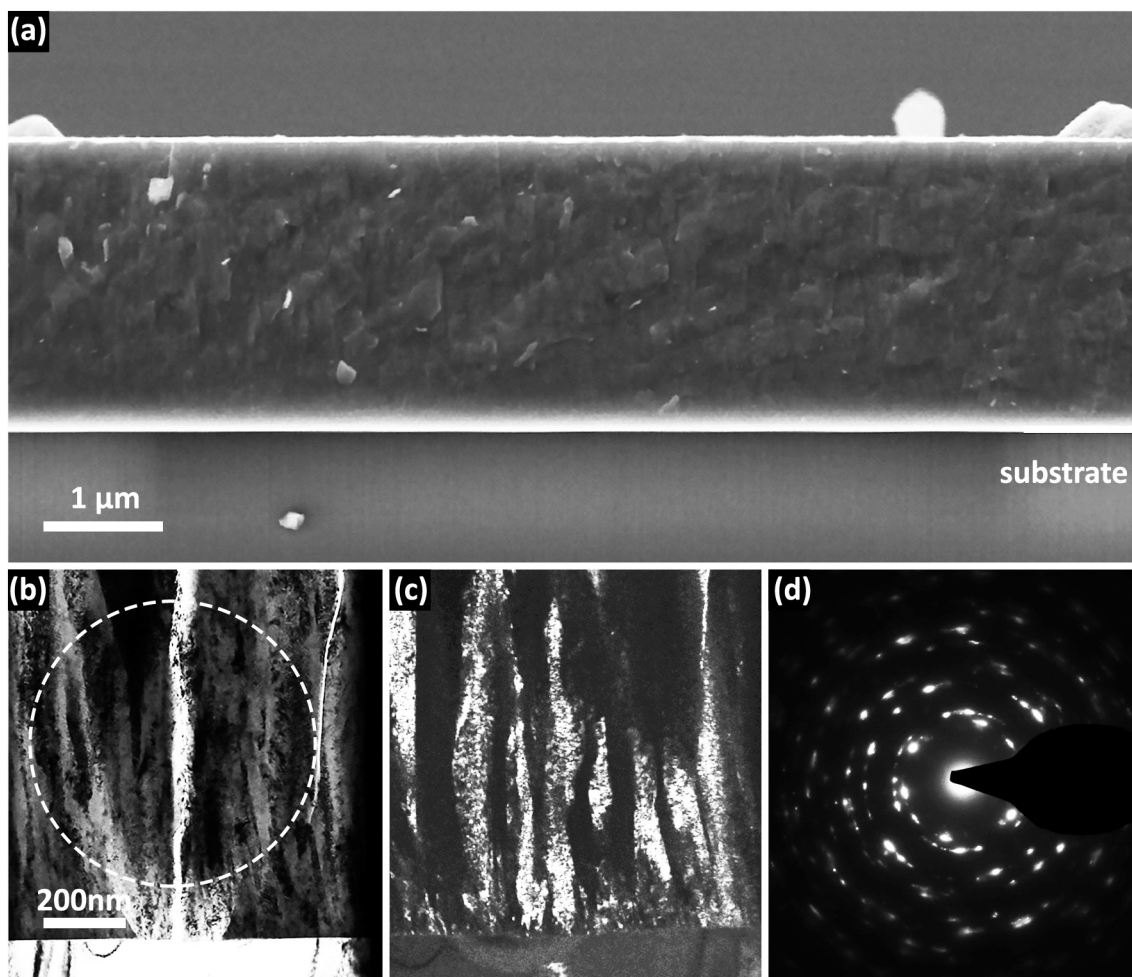


Fig. 3. Morphology of nr-(Hf,Ta,Ti,V,Zr) carbide coatings. (a) SEM fracture cross section, (b) TEM bright field image, (c) TEM dark field image, (d) SAED pattern taken from the area marked with a white dashed circle in (b).

reactively deposited coatings also crystallise in a single-phase fcc structure, which fits perfect to the XRDs.

The powdered free-standing coating materials were investigated by XRD in their as-deposited state as well as after vacuum annealing treatments up to 1300 °C to trace any possible structural changes and decomposition phenomena. The XRDs of nr-(Hf,Ta,Ti,V,Zr)C show rather symmetric peaks, see Fig. 4a. With increasing annealing temperature, a clear decrease of the full-width at half maximum (FWHM) can be observed indicating grain growth and recovery of lattice defects but no decomposition of the solid solution. Contrary to the non-reactively sputtered film, the reactively sputtered one shows asymmetric XRD peaks that could stem from the formation of an amorphous grain-boundary phase—XRD bumps from the amorphous phase could overlap with the XRD peaks from the crystalline phase—or the formation of specific lattice defects (like stacking faults, dislocation cells or walls), see Fig. 4b. Due to the powdered state, the (111) and (200) peaks are comparable in intensity, like for the non-reactively prepared film, although the film showed a pronounced 111-oriented growth (when having the material still at the substrate, compare Fig. 4a and 2a). The annealing treatment causes the formation of more symmetric XRD peaks, indicating a reduction of any amorphous phase content and/or reduction of the specific lattice defects. Like for the non-reactively prepared coatings, there are no indications for a decomposition of the solid solution fcc phase up to 1300 °C. A similar thermal stability was observed in previous studies on high-entropy metal-sublattice nitrides with the same elements on the metal-sublattice like the (Hf,Ta,Ti,V,Zr)-carbides [23].

Samples of r-(Hf,Ta,Ti,V,Zr)C as well as nr-(Hf,Ta,Ti,V,Zr)C coatings on sapphire substrate (in their as-deposited state and after vacuum annealing at temperatures up to 1300 °C) were used for nanoindentation measurements to determine the thermal stability of their mechanical properties. Unfortunately, the samples with reactively sputtered coatings could not be measured due to massive spallation, indicating that the reactive process leads to a weak interface between substrate and coating. Therefore, only the results for the non-reactively sputtered coatings are presented in Fig. 5.

In the as-deposited state, the nr-(Hf,Ta,Ti,V,Zr)C coating provides a hardness of 41.6 ± 1.6 GPa, which sometimes is named as being superhard (for $H \geq 40$ GPa [39]). The respective indentation modulus is with 438 ± 16 GPa in the range of similar non-reactively synthesised coatings as well as DFT calculated values [9,40,41]. This increased hardness, compared to the reactively sputtered coating, stems from the slightly different deposition conditions as this coating was prepared in a facility with a lower target-to-substrate distance, yielding a higher plasma density. Upon annealing at 1000 °C the hardness only slightly decreases to 40.4 ± 2.0 GPa and remains there upon a further increase in T_a to even 1200 °C. Annealing at $T_a = 1300$ °C leads to a decrease to 34 ± 2.4 GPa, which is still rather high when compared to nitrides experiencing the same annealing treatment. Similar to the hardness, the indentation modulus stays almost unaffected by the annealing treatment up to $T_a = 1200$ °C. However, increasing T_a to 1300 °C leads to an increase of the indentation modulus to 469 ± 30 GPa. This slight increase (values are still within the error bars) might stem from the densification of under-dense grain boundary regions as well as grain growth.

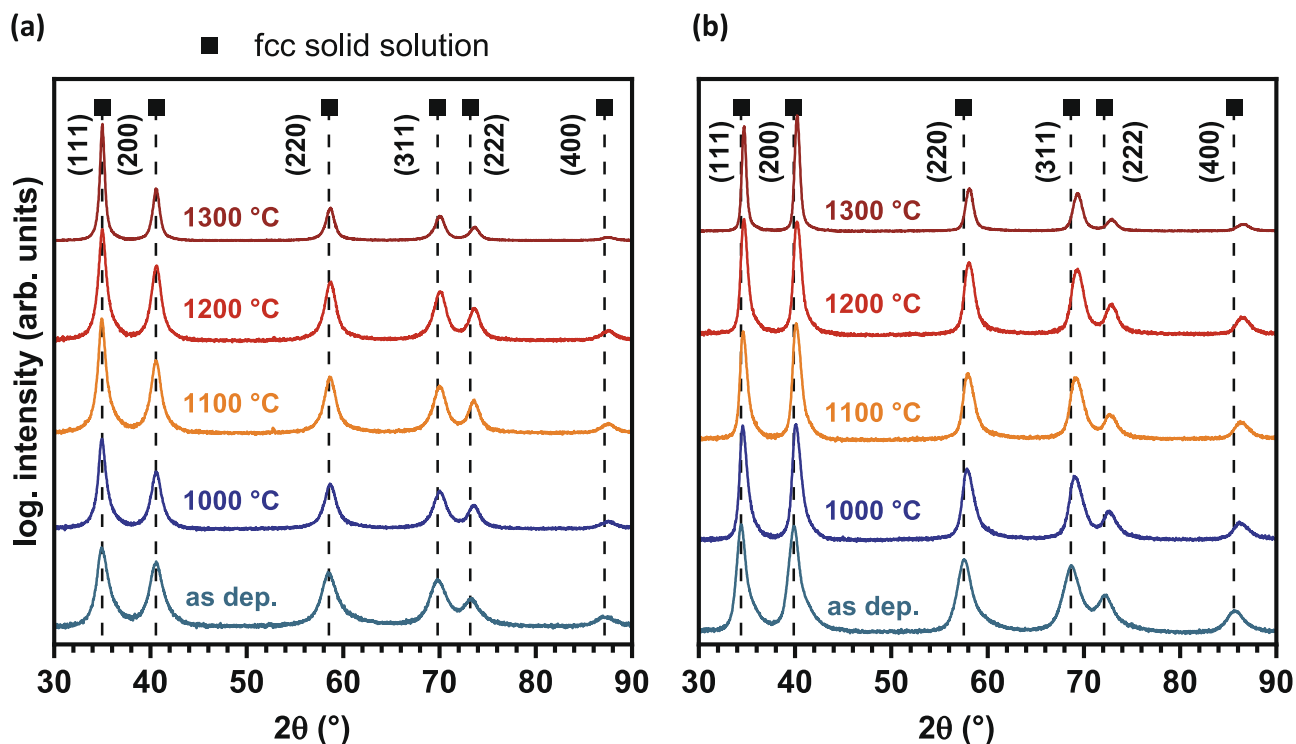


Fig. 4. XRD patterns of the powders after vacuum annealing of (a) nr-(Hf,Ta,Ti,V,Zr)C, and (b) r-(Hf,Ta,Ti,V,Zr)C.

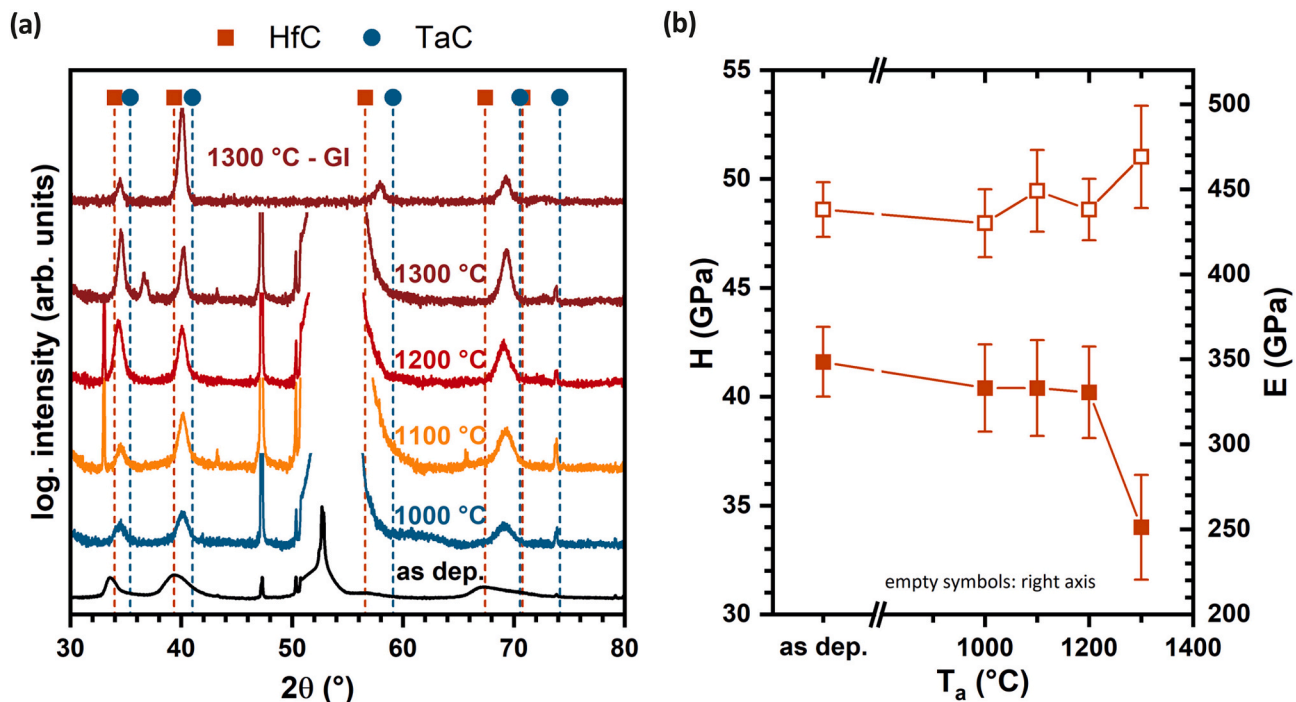


Fig. 5. (a) XRD patterns of nr-(Hf,Ta,Ti,V,Zr)C coatings on sapphire substrates after vacuum annealing with an additional grazing incidence (GI) measurement for the sample annealed at 1300 °C, and (b) hardness and indentation modulus of nr-(Hf,Ta,Ti,V,Zr)C coatings depending on the annealing temperature.

Although the XRD patterns of the annealed powdered free-standing samples have been presented above, we again show the impact of the annealing treatment on the XRD patterns (Fig. 5b), but from the samples that have been used for nanoindentation (thus, from coatings on sapphire). While the overall behaviour is very comparable to the powdered free-standing coating material, compare Fig. 4a, an additional XRD peak at $\sim 36^\circ$ can be detected for the 1300 °C annealed sample. As this is

clearly absent for the powdered free-standing coating material and the pattern obtained by a grazing incidence measurement, this peak can be attributed to a phase stemming from an interface reaction between the carbide film and the sapphire substrate. Based on existing reference patterns this phase could be a type of Al_4CO_4 (PDF #00-048-1583) with a chemical variation.

4. Summary and conclusion

(Hf,Ta,Ti,V,Zr) carbide coatings were developed using reactive and non-reactive magnetron sputtering. The coatings exhibit a single-phase fcc structure for the non-reactive process as well as for the reactive when using an acetylene flow rate ratio of 20 %. For lower acetylene flow rate ratios, the coatings also contain metallic or partly amorphous phases. The hardness of the single-phase fcc structured coating is 34.8 ± 1.6 GPa when prepared reactively and 41.6 ± 1.6 GPa when prepared non-reactively. Upon annealing powdered free-standing coating material up to 1300 °C, no decomposition can be detected via XRD. However, when annealing coated sapphire substrates, an additional XRD peak for the 1300 °C annealed sample, hints towards the formation of an interface reaction between nr-(Hf,Ta,Ti,V,Zr)C and sapphire. The r-(Hf,Ta,Ti,V,Zr)C experienced spallation during this treatment. Nanoindentation experiments after these annealing treatments showed stable values for nr-(Hf,Ta,Ti,V,Zr)C up to $T_a = 1200$ °C, a reduction in H to 34 ± 2.4 GPa and an increase in E to 469 ± 30 GPa when annealed at 1300 °C. Based on our results we can conclude, that the coating is thermally very stable (corresponding to the equivalent high-entropy sublattice nitride). As the high-entropy sublattice carbide as well as its nitride variant maintain their single-phase fcc structure and hardness up to annealing temperatures of 1200 °C (without noticeable changes), their high-entropy metal-sublattice seems to be responsible for the retarded diffusion. This together with the fact that all of the involved metals are good carbide formers highlights, that choosing the metal elements wisely is the prerequisite for enhanced properties of high-entropy metal sublattice carbides.

CRedit authorship contribution statement

A. Kirnbauer: Writing – original draft, Visualization, Methodology, Investigation, Data curation, Conceptualization. **B.I. Hajas:** Writing – review & editing, Data curation. **S. Kolozsvári:** Writing – review & editing, Resources. **P.H. Mayrhofer:** Writing – review & editing, Supervision, Resources, Project administration, Funding acquisition.

Declaration of competing interest

The authors declare that they have no known competing financial interests or personal relationships that could have appeared to influence the work reported in this paper.

Acknowledgments

The authors acknowledge the use of the X-ray center (XRC) and USTEM at TU Wien. They are also very grateful to Plansee Composite Materials GmbH for financial support. Furthermore, the authors are very grateful to Tomasz Wojcik (TU Wien, Austria) for assistance with TEM investigations and valuable discussions. The authors also acknowledge TU Wien Bibliothek for financial support through its Open Access Funding Programme.

Data availability

Data will be made available on request.

References

- P. Panjan, B. Navinšek, A. Cvelbar, A. Zalar, I. Milošev, Oxidation of TiN, ZrN, TiZrN, CrN, TiCrN and TiN/CrN multilayer hard coatings reactively sputtered at low temperature, *Thin Solid Films* 281–282 (1996) 298–301, [https://doi.org/10.1016/0040-6090\(96\)08663-4](https://doi.org/10.1016/0040-6090(96)08663-4).
- D. Panda, S.K. Sarangi, A.K. Satapathy, Influence of characteristics of flow control valves on the cooling performance of a GM cryocooler, *Vacuum* 168 (2019) 108836, <https://doi.org/10.1016/j.vacuum.2019.108836>.
- P.H. Mayrhofer, R. Rachbauer, D. Holec, F. Rovere, J.M. Schneider, Protective transition metal nitride coatings, Elsevier (2014), <https://doi.org/10.1016/B978-0-08-096532-1.00423-4>.
- P.H. Mayrhofer, A. Hörling, L. Karlsson, J. Sjölen, T. Larsson, C. Mitterer, L. Hultman, Self-organized nanostructures in the Ti–Al–N system, *Appl. Phys. Lett.* 83 (2003) 2049–2051, <https://doi.org/10.1063/1.1608464>.
- D. Edström, D.G. Sangiovanni, L. Hultman, I. Petrov, J.E. Greene, V. Chirita, Elastic properties and plastic deformation of TiC- and VC-based pseudobinary alloys, *Acta Mater.* 144 (2018) 376–385, <https://doi.org/10.1016/j.actamat.2017.10.047>.
- H. Liang, L. Fang, S. Guan, F. Peng, Z. Zhang, H. Chen, W. Zhang, C. Lu, Insights into the bond behavior and mechanical properties of hafnium carbide under high pressure and high temperature, *Inorg. Chem.* 60 (2021) 515–524, <https://doi.org/10.1021/acs.inorgchem.0c02800>.
- A. Kirnbauer, A. Wagner, V. Moraes, D. Primetzhofer, M. Hans, J.M. Schneider, P. Polcik, P.H. Mayrhofer, Thermal stability and mechanical properties of sputtered (Hf,Ta,V,W,Zr)-diborides, *Acta Mater.* 200 (2020) 559–569, <https://doi.org/10.1016/j.actamat.2020.09.018>.
- X. Gu, L. Yang, X. Ma, X. Dai, J. Wang, M. Wen, K. Zhang, Ta addition effects on the structure, mechanical and thermal properties of sputtered Hf-Ta-C film, *Ceram. Int.* 45 (2019) 15596–15602, <https://doi.org/10.1016/j.ceramint.2019.05.069>.
- H. Lasfargues, T. Glechner, C.M. Koller, V. Paneta, D. Primetzhofer, S. Kolozsvári, D. Holec, H. Riedl, P.H. Mayrhofer, Non-reactively sputtered ultra-high temperature Hf-C and ta-C coatings, *Surf. Coat. Technol.* 309 (2017) 436–444, <https://doi.org/10.1016/j.surfcoat.2016.11.073>.
- L. Chen, D. Holec, Y. Du, P.H. Mayrhofer, Influence of Zr on structure, mechanical and thermal properties of Ti–Al–N, *Thin Solid Films* 519 (2011) 5503–5510, <https://doi.org/10.1016/j.tsf.2011.03.139>.
- S.A. Glatz, H. Bolvardi, S. Kolozsvári, C.M. Koller, H. Riedl, P.H. Mayrhofer, Arc evaporated W-alloyed Ti–Al–N coatings for improved thermal stability, mechanical, and tribological properties, *Surf. Coat. Technol.* 332 (2017) 275–282, <https://doi.org/10.1016/j.surfcoat.2017.05.097>.
- S.A. Glatz, V. Moraes, C.M. Koller, H. Riedl, H. Bolvardi, S. Kolozsvári, P. H. Mayrhofer, Effect of Mo on the thermal stability, oxidation resistance, and tribo-mechanical properties of arc evaporated Ti–Al–N coatings, *J. Vac. Sci. Technol. A Vacuum, Surfaces, Film.* 35 (2017) 061515, <https://doi.org/10.1116/1.5009743>.
- R. Hollerweger, H. Riedl, J. Paulitsch, M. Arndt, R. Rachbauer, P. Polcik, S. Primig, P.H. Mayrhofer, Origin of high temperature oxidation resistance of Ti–Al–ta-N coatings, *Surf. Coat. Technol.* 257 (2014) 78–86, <https://doi.org/10.1016/j.surfcoat.2014.02.067>.
- P.H. Mayrhofer, S. Kagerer, P. Polcik, A. Kirnbauer, Superior oxidation resistance of the chemically complex but structurally simple Ti–Al–ta–Ce–Si–La–B–nitride, *Mater. Des.* 227 (2023) 111722, <https://doi.org/10.1016/j.matdes.2023.111722>.
- S. PalDey, S.C. Deevi, Single layer and multilayer wear resistant coatings of (Ti,Al)N: A review, *Mater. Sci. Eng. A* 342 (2003) 58–79, [https://doi.org/10.1016/S0921-5093\(02\)00259-9](https://doi.org/10.1016/S0921-5093(02)00259-9).
- R. Rachbauer, D. Holec, P.H. Mayrhofer, Increased thermal stability of Ti–Al–N thin films by ta alloying, *Surf. Coat. Technol.* 211 (2012) 98–103, <https://doi.org/10.1016/j.surfcoat.2011.07.009>.
- Y. Tanaka, T.M. Gür, M. Kelly, S.B. Hagstrom, T. Ikeda, K. Wakihira, H. Satoh, Properties of (Ti1–xAlx)N coatings for cutting tools prepared by the cathodic arc ion plating method, *J. Vac. Sci. & Technol. A* 10 (1992) 1749–1756, <https://doi.org/10.1116/1.577742>.
- Y.X. Xu, L. Chen, F. Pei, J.L. Yue, Y. Du, Thermal stability and oxidation resistance of V-alloyed TiAlN coatings, *Ceram. Int.* 44 (2018) 1705–1710, <https://doi.org/10.1016/j.ceramint.2017.10.100>.
- H. Asanuma, F.F. Klimashin, P. Polcik, S. Kolozsvári, H. Riedl, P.H. Mayrhofer, Impact of lanthanum and boron on the growth, thermomechanical properties and oxidation resistance of Ti–Al–N thin films, *Thin Solid Films* 688 (2019) 137239, <https://doi.org/10.1016/j.tsf.2019.04.014>.
- H. Asanuma, F.F. Klimashin, P. Polcik, S. Kolozsvári, H. Riedl, P.H. Mayrhofer, Hard Ti–Al–N endowed with high heat-resistance through alloying with ta and Ce, *Surf. Coat. Technol.* 372 (2019) 26–33, <https://doi.org/10.1016/j.surfcoat.2019.05.018>.
- H. Asanuma, F.F. Klimashin, P. Polcik, S. Kolozsvári, H. Riedl, P.H. Mayrhofer, Thermomechanical properties and oxidation resistance of Ce–Si alloyed Ti–Al–N thin films, *Vacuum* 166 (2019) 231–238, <https://doi.org/10.1016/j.vacuum.2019.05.016>.
- A. Kirnbauer, C. Spadt, C.M. Koller, S. Kolozsvári, P.H. Mayrhofer, High-entropy oxide thin films based on Al–Cr–Nb–ta–Ti, *Vacuum* 168 (2019) 108850, <https://doi.org/10.1016/j.vacuum.2019.108850>.
- A. Kirnbauer, A. Kretschmer, C.M. Koller, T. Wojcik, V. Paneta, M. Hans, J. M. Schneider, P. Polcik, P.H. Mayrhofer, Mechanical properties and thermal stability of reactively sputtered multi-principal-metal Hf-ta-Ti-V-Zr nitrides, *Surf. Coat. Technol.* 389 (2020) 125674, <https://doi.org/10.1016/j.surfcoat.2020.125674>.
- A. Kretschmer, A. Kirnbauer, V. Moraes, D. Primetzhofer, K. Yalamanchili, H. Rudigier, P.H. Mayrhofer, Improving phase stability, hardness, and oxidation resistance of reactively magnetron sputtered (Al,Cr,Nb,Ta,Ti)N thin films by Si-alloying, *Surf. Coat. Technol.* 416 (2021) 127162, <https://doi.org/10.1016/j.surfcoat.2021.127162>.
- C.H. Lai, K.H. Cheng, S.J. Lin, J.W. Yeh, Mechanical and tribological properties of multi-element (AlCrTaTiZr)N coatings, *Surf. Coat. Technol.* 202 (2008) 3732–3738, <https://doi.org/10.1016/j.surfcoat.2008.01.014>.
- H. Wang, S. Wang, Y. Cao, W. Liu, Y. Wang, Oxidation behaviors of (Hf_{0.25}Zr_{0.25}Ta_{0.25}Nb_{0.25})C and (Hf_{0.25}Zr_{0.25}Ta_{0.25}Nb_{0.25})C–SiC at

- 1300–1500 °C, *J. Mater. Sci. Technol.* 60 (2021) 147–155, <https://doi.org/10.1016/j.jmst.2020.05.037>.
- [27] P.K. Huang, J.W. Yeh, Inhibition of grain coarsening up to 1000 °C in (AlCrNbSiTiV)N superhard coatings, *Scr. Mater.* 62 (2010) 105–108, <https://doi.org/10.1016/j.scriptamat.2009.09.015>.
- [28] V. Braic, M. Balaceanu, M. Braic, A. Vladescu, S. Panseri, A. Russo, Characterization of multi-principal-element (TiZrNbHfTa)N and (TiZrNbHfTa)C coatings for biomedical applications, *J. Mech. Behav. Biomed. Mater.* 10 (2012) 197–205, <https://doi.org/10.1016/j.jmbbm.2012.02.020>.
- [29] E. Castle, T. Csanádi, S. Grasso, J. Dusza, M. Reece, Processing and properties of high-entropy ultra-high temperature carbides, *Sci. Rep.* 8 (2018), <https://doi.org/10.1038/s41598-018-26827-1>.
- [30] T.J. Harrington, J. Gild, P. Sarker, C. Toher, C.M. Rost, O.F. Dippo, C. McElfresh, K. Kaufmann, E. Marin, L. Borowski, P.E. Hopkins, J. Luo, S. Curtarolo, D. W. Brenner, K.S. Vecchio, Phase stability and mechanical properties of novel high entropy transition metal carbides, *Acta Mater.* 166 (2019) 271–280, <https://doi.org/10.1016/j.actamat.2018.12.054>.
- [31] M.D. Hossain, T. Borman, C. Oses, M. Esters, C. Toher, L. Feng, A. Kumar, W. G. Fahrenholtz, S. Curtarolo, D. Brenner, J.M. LeBeau, J.P. Maria, Entropy landscaping of high-entropy carbides, *Adv. Mater.* 33 (2021), <https://doi.org/10.1002/adma.202102904>.
- [32] P. Sarker, T. Harrington, C. Toher, C. Oses, M. Samiee, J.P. Maria, D.W. Brenner, K. S. Vecchio, S. Curtarolo, High-entropy high-hardness metal carbides discovered by entropy descriptors, *Nat. Commun.* 9 (2018), <https://doi.org/10.1038/s41467-018-07160-7>.
- [33] J. Pötschke, M. Dahal, M. Herrmann, A. Vornberger, B. Matthey, A. Michaelis, Preparation of high-entropy carbides by different sintering techniques, *J. Mater. Sci.* 56 (2021) 11237–11247, <https://doi.org/10.1007/s10853-021-06004-y>.
- [34] Y. Wang, Processing and properties of high entropy carbides, *Adv. Appl. Ceram.* 121 (2022) 57–78, <https://doi.org/10.1080/17436753.2021.2014277>.
- [35] J. Zhou, J. Zhang, F. Zhang, B. Niu, L. Lei, W. Wang, High-entropy carbide: a novel class of multicomponent ceramics, *Ceram. Int.* 44 (2018) 22014–22018, <https://doi.org/10.1016/j.ceramint.2018.08.100>.
- [36] W.C. Oliver, G.M. Pharr, An improved technique for determining hardness and elastic modulus using load and displacement sensing indentation experiments, *J. Mater. Res.* 7 (1992) 1564–1583.
- [37] A. Krajewski, L. D'Alessio, G. De Maria, Physico-chemical and Thermophysical properties of cubic binary carbides, *Cryst. Res. Technol.* 33 (1998) 341–374. <http://api.semanticscholar.org/CorpusID:98037421>.
- [38] P.H. Mayrhofer, M. Geier, C. Löcker, L. Chen, Influence of deposition conditions on texture development and mechanical properties of TiN coatings, *Int. J. Mater. Res.* 100 (2009) 1052–1058, <https://doi.org/10.3139/146.110159>.
- [39] S. Vepřek, S. Reiprich, A concept for the design of novel superhard coatings, *Thin Solid Films* 268 (1995) 64–71, [https://doi.org/10.1016/0040-6090\(95\)06695-0](https://doi.org/10.1016/0040-6090(95)06695-0).
- [40] T. Glechner, S. Lang, R. Hahn, M. Alfreider, V. Moraes, D. Primetzhofer, J. Ramm, S. Kolozsvári, D. Kiener, H. Riedl, Correlation between fracture characteristics and valence electron concentration of sputtered Hf-C-N based thin films, *Surf. Coat. Technol.* 399 (2020) 126212, <https://doi.org/10.1016/j.surfcoat.2020.126212>.
- [41] T. Glechner, R. Hahn, T. Wojcik, D. Holec, S. Kolozsvári, H. Zaid, S. Kodambaka, P. H. Mayrhofer, H. Riedl, Assessment of ductile character in superhard ta-C-N thin films, *Acta Mater.* 179 (2019) 17–25, <https://doi.org/10.1016/j.actamat.2019.08.015>.